Vietnam Journal of Science and Technology ***62*** *(2024)*

doi:10.15625/2525-2518/18507

Green synthesis of nanostructured 1T/2H-MoS_2 hybrid phase with polyol solvents and microwave heating

Nguyen Thi Minh Nguyet[1, 2,*], Vuong Vinh Dat[2, 3], Nguyen Huu Huy Phuc[2, 3], Le Van Thang[1, 2]

[1]*VNU-HCM Key Laboratory for Material Technologies, Ho Chi Minh City University of Technology (HCMUT), 268 Ly Thuong Kiet Street, Ward 14, District 10, Ho Chi Minh City, Viet Nam*

[2]*Vietnam National University Ho Chi Minh City, Linh Trung Ward, Thu Duc District, Ho Chi Minh City, Viet Nam*

[3]*Faculty of Materials Technology, Ho Chi Minh City University of Technology (HCMUT), 268 Ly Thuong Kiet Street, Ward 14, District 10, Ho Chi Minh City, Viet Nam*

[*]Emails: *minhnguyet@hcmut.edu.vn*

Received: 12 July 2023; Accepted for publication28 March 2024

Abstract. Green synthesis approaches have attracted greatly of attention in recent years since they address the issues associated with sustainability than conventional synthesis methods. New research fields in green nanoscience are being developed as a result of the incorporation of green chemistry principles into nanoscience. In this paper, the successful microwave-assisted green synthesis of MoS_2 nanoparticles in a single pot using polyol solvents such as ethylene glycol and glycerol is demonstrated. The coexistence of 1T and 2H phases in MoS_2 nanomaterials was determined using advanced techniques such as XRD, Raman, XPS, and TEM images. The highest 1T proportion obtained was 84.5 % when compared to the 2H phase. The reaction mechanism and the phase transition between 1T and 2H were described and illustrated. The role of polyol solvents in the practical synthesis of nano MoS_2 under microwave heating is also evaluated and explained. Due to the ability of the metallic 1T phase to enhance electrical conductivity, it is believed that hybrid nanostructures exhibit superior electrochemical performance for energy storage and conversion applications.

Keywords: nano MoS_2, hybrid phase 1T/2H-MoS_2, polyol solvents, microwave synthesis, green chemistry

Classification numbers: 2.4.2, 2.4.4, 5.2.1

1. INTRODUCTION

The metastable form of metallic 1T phase in nano molybdenum disulfide (MoS2) has shown promise in enhancing electron transport and ion diffusion for electrochemical energy storage technologies [2 - 12]. Compared to the semiconducting 2H-MoS_2, the 1T-MoS_2 exhibits superior properties such as a larger interlayer distance, a higher electronic conductivity, and chemical activity. However, its stability remains a challenge [13]. When a partial

transformation from the 2H to the 1T phase occurs in the 1T/2H-MoS_2 mixed-phase heterostructure, the kinetic barrier decreases, and more electron transfer occurs, resulting in an increased number of active sites, which significantly increases its catalytic activity [6, 12, 14 - 16]. The hybrid nanostructures of 1T and 2H phases exhibit excellent electrochemical properties, including large specific capacitance, super high-rate capability, and excellent long-cycle durability, making them a promising electrode material for supercapacitor devices [7, 17].

Recently, there has been an increased focus on synthesizing nanomaterials using environmentally friendly methods, often referred to as green synthesis or green chemistry [18-20]. The principles of green chemistry and energy efficiency are becoming increasingly important, driving industry towards commercializing microwave technology [21]. Green methods using microwave heating and ultrasonic techniques are employed due to their simplicity, lower cost, and higher reproducibility [22, 23] . In microwave processing, heat is generated at the interface between polar and polarized components (i.e. water and other solvent mixtures). Heat transfers via conduction enable materials to achieve optimal energy levels [24]. Furthermore, mass and heat are transported along the same channel, resulting in a synergistic effect that promotes analyte recovery. This is one of the benefits of adopting the microwave-assisted technique; it moderates the extraction time and solvent volume, which other procedures do not. Solvents play a crucial role in microwave-assisted synthesis in the liquid phase. The choice of solvent is a crucial factor for the microwave-assisted formation of inorganic nanostructures. Ethylene glycol (EG) and glycerol (G) are two commonly used polyols for the synthesis of nano MoS_2 due to their high boiling points, microwave compatibility, appropriate viscosity, and ability to promote nanoparticle nucleation and development. The high boiling points of polyols enable synthesis at temperatures ranging from 200 to 320 °C without high pressure or autoclaves [25 - 27].

This study aims to investigate the effectiveness of the green microwave technique in producing 1T/2H-MoS_2 nanomaterials using polyol solvents. The paper presents a thorough analysis of the structural and property characteristics of the synthesized materials and elucidates the underlying chemical mechanism that governs the formation of hybrid-phase nanostructures. Additionally, the role of polyol solvents in the practical synthesis of nano MoS_2 under microwave heating is evaluated and explained. The metallic 1T phase's ability to enhance electrical conductivity suggests that hybrid nanostructures may exhibit superior electrochemical performance for energy storage and conversion applications. The successful green synthesis of MoS_2 nanoparticles using polyol solvents and microwave heating provides a more sustainable and efficient approach to nanomaterial synthesis, with potential applications in various fields.

2. MATERIALS AND METHODS

To synthesize nano MoS_2, 1.24 g (0.001 mol) of ammonium heptamolybdate tetrahydrate (AHM) $(NH_4)_6Mo_7O_{24}.4H_2O$ and 2.28 g (0.03 mol) of thiourea (TU) CSN_2H_4 were immersed in 60 mL of various solvents and kept on a hot plate at 60 ^oC for 30 minutes. In this study, three solvents were investigated to synthesize nano-MoS_2: ethylene glycol (EG), glycerol (G), and ethylene glycol mixed with glycerol (EG + G) in a volume ratio of 1:1, and. The homogeneous solution was then placed in a microwave oven. The reaction mixture was rapidly heated to the boiling points of the solvents and mixing solvents, and the microwave irradiation power was held constant at 240 W for 15 minutes. The reaction mixture was cooled to room temperature and diluted with ethanol when a significant amount of black precipitate formed. The black precipitates were collected using centrifugation and then filtered and washed several times with

ethanol. Finally, the powder was vacuum dried for 5 hours at 80 ^{o}C. The final MoS_2 nanostructure samples were labeled S1-EG, S2-EG +G, and S3 - G.

In this work, X-ray diffraction (XRD) measurements are performed on a Bruker D8 Advance diffractometer with Cu K radiation (Institute of Applied Materials Science, VAST). The diffraction was performed from 5 ^{o} to 80 ^{o} at a scan rate of 1° min^{-1} and a step size of 0.0194 °. The structure information for the as-prepared materials was obtained using a Labram HR VIS Mico Raman spectrometer at room temperature with a He-Ne excitation wavelength of 632.8 nm on a 300 lines/mm grating. The laser power was kept at 1 mW to avoid the oxidation effect on the MoS_2 samples. The morphology and structure of the prepared samples were analyzed by transmission electron microscopy (TEM) (JEOL-TEM-1400) at the National Key Laboratory of Polymer and Composite Materials (PCKLABS) at Ho Chi Minh City University of Technology. The equipment operated at an acceleration voltage of 200 kV in the bright field image mode. Important information on the surface electronic state and the composition of the final product can be provided by XPS. The synthesized MoS_2 nanopowders were analyzed through an X-ray photoelectron spectroscopy (XPS) ESCALAB250 system with Al (K) radiation as the probe under vacuum. A survey scan was performed over a wide binding energy range of 0-1000 eV for a detailed analysis of Mo and S elements, focusing on the appropriate and specific energy windows. The energies of C 1s peak at 284.6 eV to calibrate the samples' binding energies. Meanwhile, the values of full width at half maximum (FWHM) were kept equal between the spin-orbit splitting doublets.

3. RESULTS AND DISCUSSION

X-ray diffraction (XRD) analysis is a commonly used technique to determine the crystal structure and size, as well as the crystalline phase and purity of a crystal. During the microwave irradiation process, intercalation and heat treatment can significantly impact the crystal structure of the host materials, resulting in a phase transition from semiconducting (2H) to metallic (1T), as seen in the XRD pattern presented in Figure 1.

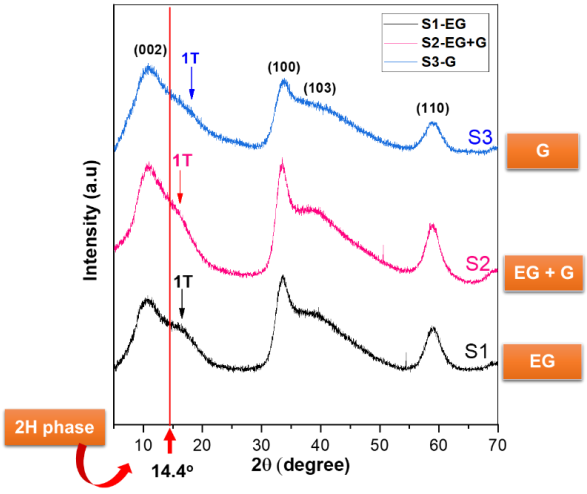

Figure 1. XRD patterns of **S1**-EG, **S2**-EG+G, and **S3**-G.

To determine the XRD spectrum of mixed-phase 1T/2H-MoS_2, a comparison with the XRD

spectrum of bulk 2H-MoS_2 is necessary [1, 28] . Figure 1 shows the XRD patterns of the three samples (S1-EG, S2-EG+G, and S3-G). All samples exhibit XRD peaks at 31.9 °, 43.3 °, and 56.8 °, which correspond to the (100), (103), and (110) planes of MoS_2, respectively. However, the characteristic peak of the (002) plane of 2H-MoS_2 at ~ 14.41 ° is absent and instead exhibits peak splitting at lower and higher 2θ angles (red dashed rectangle in Figure 1). This disordered structure matches the previously reported ammoniated 1T-MoS_2 [7], indicating the formation of a 1T/2H-MoS_2 hybrid phase. The large interlayer spacing of the as-prepared MoS_2 in those of S1-EG (2θ ~ 10.6 °), S2-EG+G (2θ ~ 10.9 °), S3-G (2θ ~ 10.9 °) is attributed to the high content of 1T-MoS_2 in these samples [29]

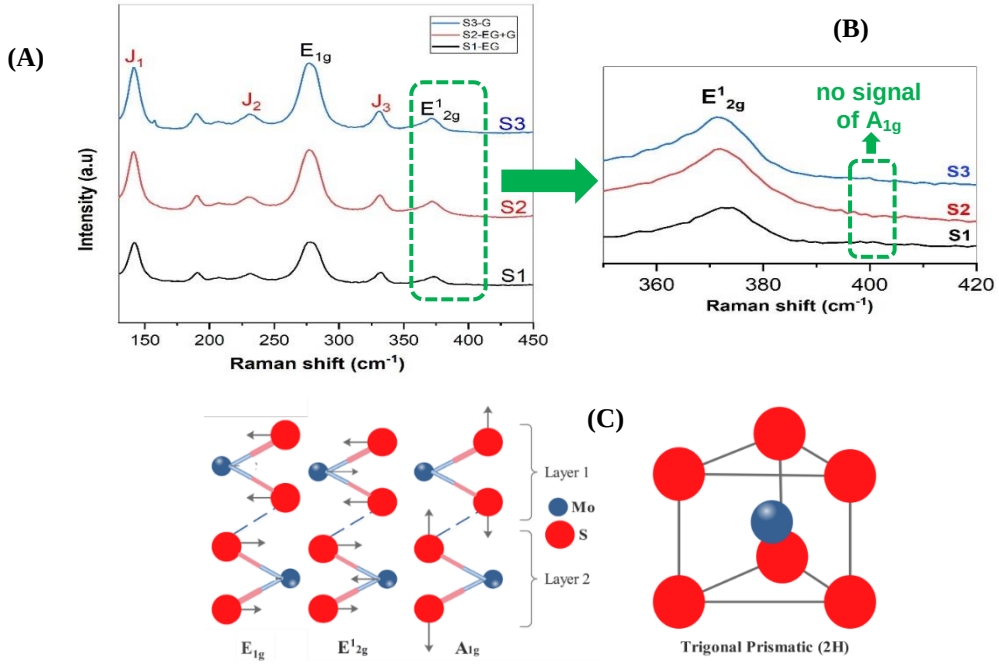

Figure 2. (A) Raman spectra of **S1**-EG, **S2**-EG+G, **S3**-G; (B) the maginified Raman signals of green area from figure (A); and (C) symmetric displacement of Mo and S atoms in E_{1g}, E^1_{2g} and A_{1g} vibrational modes.

Figure 2A displays the Raman spectra of S1-EG, S2-EG+G, and S3-G, which were synthesized using various solvents such as EG, EG+G, and glycerol (G). Table 1 summarizes the detected vibrations in all three samples. A more detailed view of the vibrational modes is presented in Figure 2C. The observed strong peaks at 141, 190, 230, and 331 cm^{-1}, which correspond to the stretching vibration of Mo–Mo and the phonon mode of 1T-MoS_2, indicate the presence of 1T-MoS_2 in all samples [1, 29, 30]. The A_{1g} to J_1 intensity ratio in a spatially resolved Raman spectra of MoS_2 can be utilized to determine the phase content, as it is inversely proportional to the amount of 1T phase present. In S1-EG, S2-EG+G, and S3-G, the J_1 peak is visible, but the A_{1g}/J_1 value is extremely low and cannot be seen in Figure 2B when zoomed in, indicating a high 1T phase content. The increase in the A_{1g}/J_1 value indicates a decrease in the 1T phase content and the formation of a mixed phase of 1T/2H [31]. This explains the absence of A_{1g} peaks in the Raman spectra of samples S1-EG, S2-EG+G, and S3-G, as shown in Figure 2B. Additionally, the low crystallinity and lack of 2H phase in the MoS_2 material may account for the significant reduction in the intensity of typical E^1_{2g} and A_{1g} peaks

over 1T/2H-MoS_2 in S1-EG, S2-EG+G, and S3-G [1, 14].

Table 1. Summarize the vibration modes (position peaks) in S1, S2, and S3 (cm^{-1})

Samples	J_1	Phonon mode	J_2	E_{1g}	J_3	E^1_{2g}	A_{1g}
S1 - EG	~141.6	~ 190	~230	~278	~331	~372	-
S2 - EG+G	~141.5	~ 190	~230	~278	~331	~372	-
S3 - G	~141.9	~ 190	~230	~278	~331	~372	-

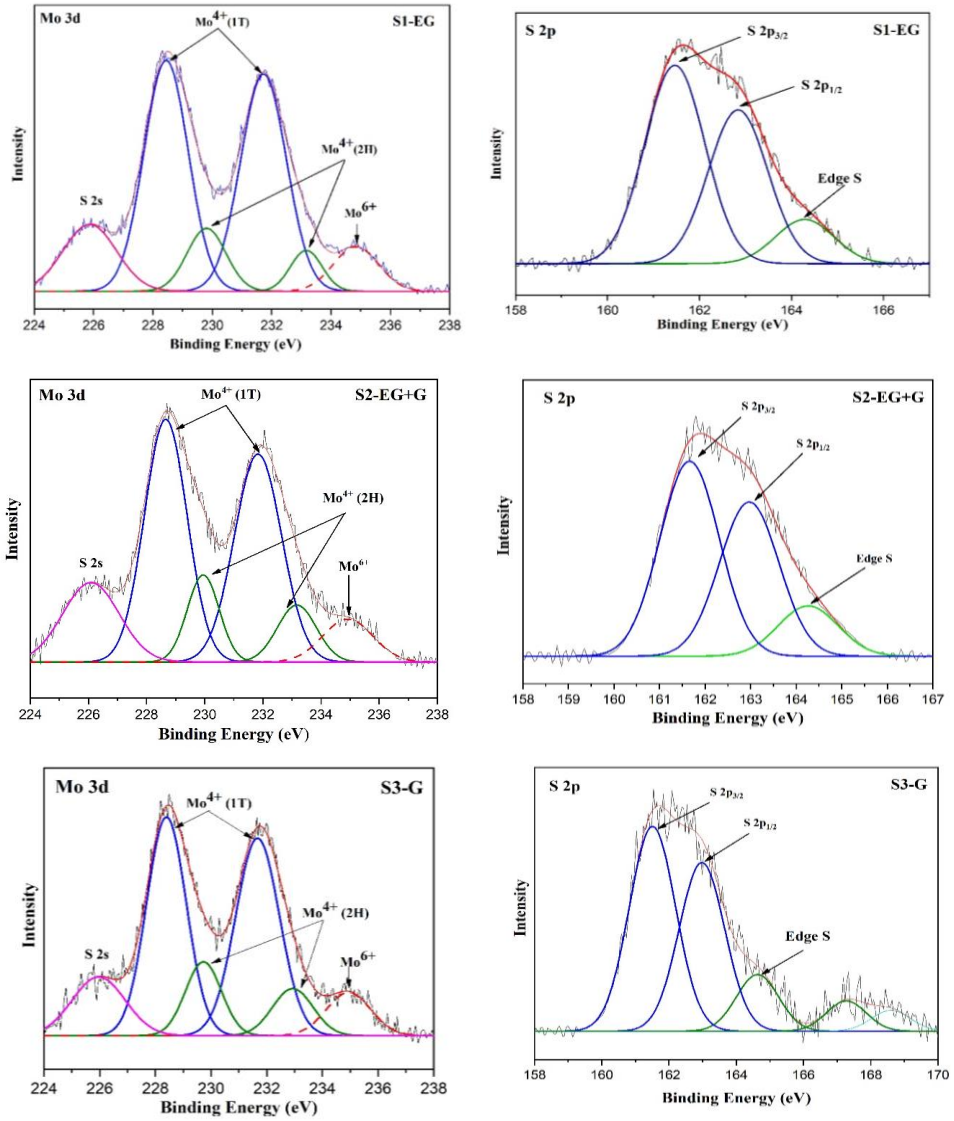

Figure 3. **Mo 3d** and **S 2s** XPS spectra of 1T/2H-MoS_2 in S1-EG, S2-EG+G , and S3-G.

The analysis of the binding energy from the peak of the Mo 3d and S 2p orbitals in typical XPS spectra of Mo 3d and S 2p orbitals proves the formation of MoS_2. The XPS data in Figure 3 have shown well-defined signals for 1T-MoS_2, 2H-MoS_2, and a small content of MoO_3 in all the

solvents investigated. The mixed-phase 1T/2H-MoS_2 material exhibits distinct atomic states for Mo and S due to its combination of trigonal prismatic (2H-MoS_2) and octahedral (1T-MoS_2) coordination structures. These different coordination structures give rise to variations in the binding energies of Mo and S. According to reports, the 3d doublet ($3d_{5/2}$ and $3d_{3/2}$) for Mo in any oxidation state has an energy separation of approximately 3.2 eV, with a characteristic peak intensity ratio of 3:2 for $3d_{5/2}$ to $3d_{3/2}$ [32]. Furthermore, it has been observed that the binding energies of 3d5/2 and 3d3/2 for all oxidation states of Mo exhibit a higher shift compared to the corresponding binding energy values for elemental Mo, which are 228 and 231.1 eV, respectively [33]. In the case of the mixed-phase 1T/2H-MoS_2 material, a peak pair (at 228.394 eV and 231.668 eV) is observed, which demonstrates a shift from the 3d doublet of elemental Mo. This shift is lower than the shift observed for Mo (IV) in 2H-MoS_2 (approximately 1.3 eV). Consequently, the peak pair at 228.394 eV and 231.668 eV can be attributed to the $3d_{5/2}$ and $3d_{3/2}$ (i.e., the 3d doublet) binding energies of Mo (IV) species in 1T-MoS_2 [3, 8, 34 - 36]. From figure 3, the two characteristic peaks around 229.803 and 233.167 eV were observed in all three samples, indicating the 2H phase of MoS_2 [1, 7, 37-39]. The binding energy of the Mo 3d peaks in 1T-MoS_2 was found to be approximately 1.3 eV lower than that in 2H-MoS_2, which is consistent with previous reports [30, 37, 40, 41]. Similarly, a downshift in the binding energies can be observed in the S 2p peaks. Peaks at 161.466 and 162.840 eV in the S 2p spectrum are attributed to S $2p_{3/2}$ and S $2p_{1/2}$ of S^{2-} in MoS_2 [42]. The increased electron density around Mo and S in 1T-MoS_2 leads to a shift in the binding energy to lower values [33]. In the Mo 3d orbitals (Figure 3), a lone peak at approximately 235 eV appears due to the presence of Mo (VI) in MoO_3. The $3d_{5/2}$ counterpart of the 3d doublet, with a binding energy of approximately 232 eV, may have merged with the broad peak at 231.611 eV. This trace amount of MoO_3 might have formed during the handling of the sample in the ambient atmosphere. Additionally, another peak at approximately 225.868 eV, often observed in the Mo 3d spectrum, can be attributed to the presence of the S 2s orbital, indicating the Mo-S bond in MoS_2 [40].

The relative concentration of the 1T and 2H phases in various solvents was calculated, using XPS as the ratio between the Mo 3d peak areas. Each phase's fraction was calculated following the equation (1) below and then summarized in table 2 [43]. All the MoS_2 products comprise both phases – 1T and 2H - but their compositions vary depending on the solvents (reaction temperatures). Notably, 1T phase proportion was decreased when increasing the reaction temperatures ($T_{EG} < T_{(EG+G)} < T_G$) [44]. The low temperature of MoS_2 synthesized in ethylene glycol (EG) enabled such rich composition of the 1T-phase, as 84.5% as calculated in Table 2 with added mechanical and thermal stability due to co-existence with the 2H-phase. Because of the presence of a highly conductive 1T phase rather than a 2H phase, these hybrid materials have the potential to improve the electrochemical properties of batteries or capacitors.

$$Fraction\ of\ 2H\ phase = \frac{2H\ (3d_{5/2}) + 2H\ (3d_{3/2})}{2H\ (3d_{5/2}) + 2H\ (3d_{3/2}) + 1T\ (3d_{5/2}) + 1T\ (3d_{3/2})} \times 100\% \quad (1)\ [43]$$

Table 2. 1T and 2H phase proportions in MoS_2 nanomaterials synthesized in different polyol solvents,

PHASE	PHASE FRACTION		
	S1-EG	S2 -EG+G	S3 - G
2H	15.5 %	19.8 %	20.8 %
1T	84.5 %	80.2 %	71.2 %

High-resolution TEM (HRTEM) is performed to visualize the 1T/2H crystal surface structures with lattice fringes (Figure 4). The enlarged red rectangle in Figure 4 (A), depicted in Figure 4 (B) and (C), reveals the trigonal lattice area of the 1T phase and the honeycomb lattice area of the trigonal prismatic coordination in the 2H phase. As depicted in Figure 4 (D), the interlayer distances were measured to be 0.236 nm, which is given to the d spacing of the (100) planes of the 1T phase MoS_2 [45].

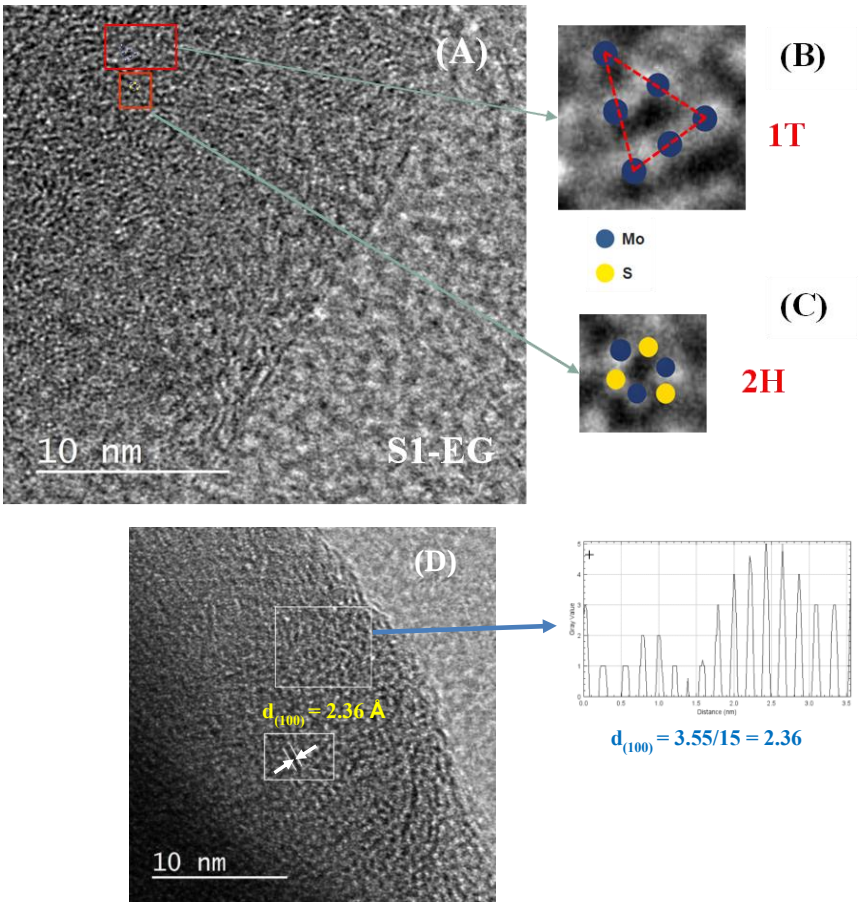

Figure 4 (A) HRTEM images of S1-EG; (B) Image of the region enclosed by the red rectangle of (A) and schematic structure of the unit cells of the 1T phase; (C) Image of the region enclosed by the red rectangle in (A) and schematic structure of the unit cells of the 2H phase; (D) measurement of interlayer distances by ImageJ to calculate the d spacing between the (100) planes of 1T phase MoS_2.

Figure 5 illustrates the formation of diverse morphologies in the MoS_2 materials. When comparing the nanoparticle morphology of the S1-EG and S3-G samples, the TEM images of the S2-EG+G sample reveal the presence of numerous nanoflake wrinkles. These wrinkles are agglomerates or aggregates composed of homogeneous MoS_2 particles or flakes. The particle boundaries are more distinct in S3-G compared to S1-EG and S2-EG+G. In S1-EG and S2-EG+G, the flakes exhibit corrugation, indicating the flexible and ultrathin nature of the material.

The integration of TEM images with XRD, Raman, and XPS data offers compelling evidence that MoS_2 materials have been successfully synthesized at the nanoscale, exhibiting diverse morphologies. Remarkably, the TEM images reveal variations in the size and shape of

metal sulfide nanoparticles, even when employing the same microwave synthesis route. These findings suggest that microwave irradiation can selectively influence the nucleation and growth rates of distinct compounds.

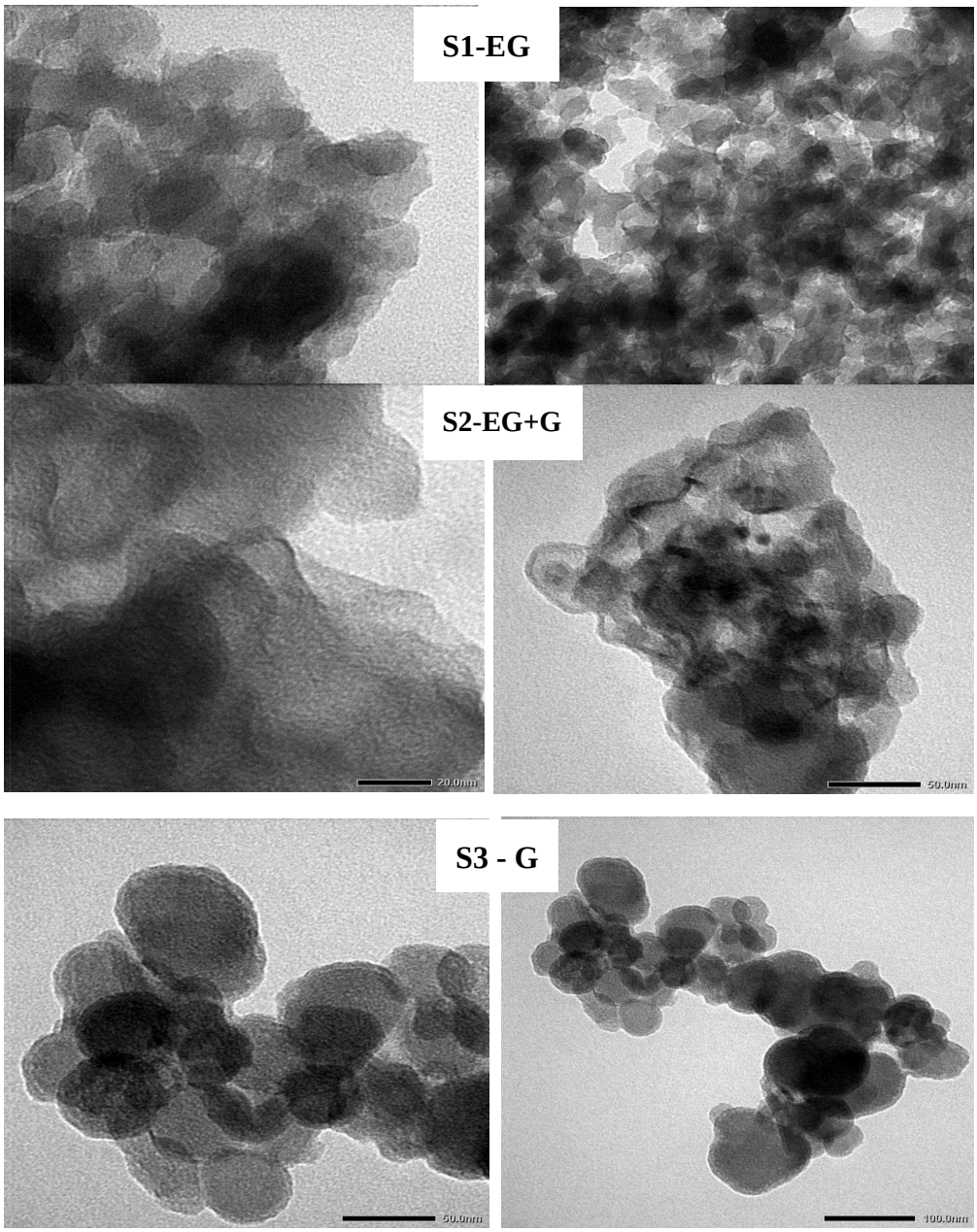

Figure 5 TEM images of 1T/2H-MoS_2 in S1-EG, S2-EG+G and S3-G.

Explain the mechanism for synthesis reaction and propose the structure of as-prepared material

The probable mechanism of the reaction of microwave heating synthesis of 1T/2H-MoS_2 nanoparticles is presented by the following steps:

(1) Dissociation: Two types of water are present in the precursor: structural water, which is bound chemically and is an integral part of $(NH_4)_6(Mo_7O_{24}) \cdot 4H_2O$, and water present in ethylene glycol. Microwave-induced dissociation reactions of AHM and TU species in polyol solvents are likely to occur as the following equations:

$$(NH_4)_6(Mo_7O_{24}) \cdot 4H_2O + H_2O \rightarrow [Mo_7O_{24}]^{6-} + 6\ NH_4^+ \quad (2)$$

$$[Mo_7O_{24}]^{6-} \rightarrow 6[MoO_4]^{2-} + Mo^{6+} \quad (3)$$

$$H_2NCSNH_2 \rightarrow NH_4^+ + NCS^- \quad (4)$$

$$H_2NCSNH_2 + H_2O \rightarrow 2NH_3 + CO_2 + H_2S \quad (5)$$

(2) Nucleation: Initially, MoS_2 nanocrystal seeds are formed due to the reaction between AHM and thiourea. The nucleation process initiates the formation of a new crystalline entity from a solution. During the synthesis process, the nanocrystal seeds grow into larger crystals and gather together to form clusters, as well as new crystals, form continuously. The reactions that occur are as follows:

$$MoO_4^{2-} + H_2S + 2H_2O \rightarrow MoO_2 + SO_4^{2-} + 6H^+ \quad (6)$$

$$MoO_2 + 2H_2S \rightarrow MoS_2 + 2H_2O \quad (7)$$

(3) Crystal growth

Initially, MoS_2 nanocrystal seeds are generated due to the reaction between AHM with thiourea. The nanocrystal seeds grow into larger crystals and cluster together throughout the synthesis process while new crystals continue to form. Mo atoms and S atoms form a chemical bond along the plane direction in a monolayer MoS_2, much stronger than the Van der Waals force between two monolayers MoS_2. As a result of the ability of MoS_2 to form stable Mo-S bonds in the plane direction, massive MoS_2 flakes can be observed in clusters in various solutions such as EG, glycerol, and EG/G. Ammonium ions can penetrate the gap between the MoS_2 monolayers, resulting in a relatively small flake size and many bulk structures with a considerable layer distance. These bulk formations are thought to be generated by the aggregation of small MoS_2 flakes.

An illustrated mechanism for the growth of MoS_2 crystals involves the presence of $[Mo_7O_{24}]^{6-}$ ionic groups in a neutral solution. These groups are composed of seven octahedral $[MoO_6]$ ionic groups that contain Mo and O atoms with three different bond lengths. As NH_2CSNH_2 produces S^{2-} ions, they replace the terminal O atoms connected by the Mo–O ionic bond because the bond energy of Mo–S is higher than that of the terminal Mo–O bond [46].

Solvents play significant roles in microwave-assisted liquid-phase synthesis. Ethylene glycol (EG) and glycerol (G) have a high boiling point (>180 ^oC), are microwave-compatible, have an appropriate viscosity, and promote nanoparticle nucleation and development in high boiling polyols. The nucleation and growth of nanoparticles in high boiling polyols such as ethylene glycol (EG) and glycerol are the primary reasons for their use in nano MoS_2 production. The polyol acts as both a solvent and a stabilizing agent, in this case, restricting particle growth while limiting particle agglomeration and aggregation [47].

Explain the phase transitions between 1T and 2H under microwaves irradiation

2H phase formed in the first stage and then transitioned to a 1T phase via an NH_4^+ ion-induced phase transformation, similar to intercalated Li^+ [48]. The NH^{4+} ion destabilizes the trigonal-prismatic 2H-MoS_2 structure, favoring the octahedrally coordinated 1T-MoS_2. The NH_4^+ ion destabilizes the trigonal-prismatic 2H-MoS_2 structure and favors the octahedrally coordinated 1T-MoS_2.

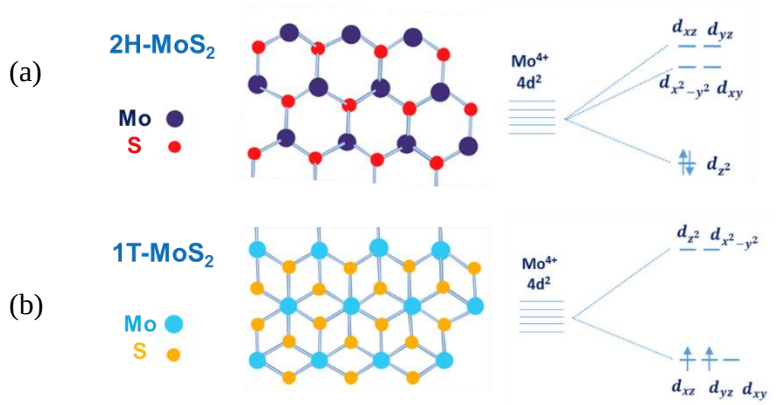

Figure 6. (a) The 2H-MoS_2 crystal structure and the ligand splitting for 4d orbitals of Mo atoms with trigonal-prismatic coordination, (b) The 1T-MoS_2 crystal structure and the ligand splitting for 4d orbitals of Mo atoms with octahedral coordination.

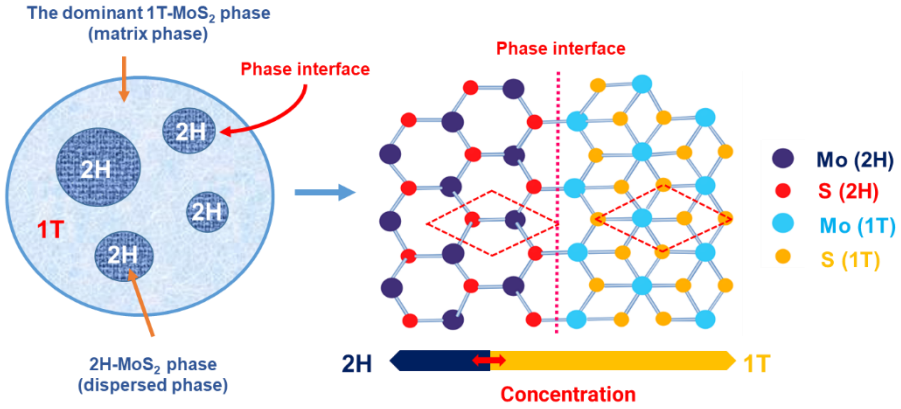

Figure 7. An illustration of the phase distribution in a 1T/2H-MoS_2 material in which the 1T is the dominant phase.

The microwave irradiation has two effects on the synthesis of 1T/2H-MoS_2. For starters, the microwave dipole rotation destroys the weak van der Waals forces between the layers of MoS_2 and increases their interlayer spacing (shift (002) peaks to lower angel in XRD patterns). Second, ammonium ions enter the MoS_2 interlayers in a non-uniform manner, making the lattice unstable for phase transition from 2H to 1T. As previously stated, there are three groups (d_{xz}, d_{yz}), (d_{xy}, $d_{x^2y^2}$), and (d_{z^2}) of electrons in the 4d orbital of Mo in the 2H phase, of which the (d_{z^2}) orbital is filled with electrons, leaving other orbitals empty and contributing to the phase structure's stability (Figure 6). After being exposed to microwave radiation, the ammonium ions in the matrix cause an electron to partially occupy the (d_{xy}, $d_{x^2y^2}$) orbital, reducing its stability and facilitating phase conversion from the 2H to the 1T phase. The electrons of Mo are occupied in two of the three degenerate orbitals in the two groups ($d_{x^2y^2}$, d_{z^2}) and (d_{xy}, d_{xz}, d_{yz}) of the

1T phase (d_{xy}, d_{xz}, d_{yz}). As a result of the three degenerate orbitals being filled, the addition of an electron increases phase stability. Because of lattice instability, the interaction between MoS_2 and ammonium ions weakens the top Mo–S bond, causing phase conversion from the 2H to 1T phase [30].

The hybrids materials in S1-EG, S2- EG+G, S3-G demonstrated that the 1T phase has a more dominating composition than the 2H phase, based on the results of computing the 1T and 2H phase compositions using XPS spectra. As a result, we refer to the phase that occupies the upper component as the matrix phase and the remaining phase as the randomly dispersed phase inside the matrix phase. Figure 7 illustrates the phase distribution of the 1T and 2H phases in the synthesized MoS_2 hybrid material.

4. CONCLUSIONS

In conclusion, the successful synthesis of 1T/2H-MoS_2 nanomaterials using a green method based on microwave heating and green solvent polyols has been demonstrated. This new approach offers several advantages over traditional synthesis methods, including shorter reaction times, lower energy consumption, and the use of environmentally friendly solvents. The use of polyol solvents including ethylene glycol (EG), ethylene glycol mixed with glycerol (G) in a volume ratio of 1:1, and glycerol (G) has been shown to be effective in controlling the phase fraction of 1T/2H MoS_2, with the highest 1T concentration reaching 84.5%. This is a significant achievement, as the 1T phase has been shown to exhibit superior electrochemical performance due to its enhanced electrical conductivity. The reaction mechanism and phase transition between the 1T and 2H phases have been described and illustrated, shedding light on the complex behavior of this hybrid material. The role of polyol solvents in the practical synthesis of nano MoS_2 under microwave heating has also been evaluated and explained.

Acknowledgements. We acknowledge Ho Chi Minh City University of Technology (HCMUT), VNU-HCM for supporting this study.

CRediT authorship contribution statement. Vinh-Dat Vuong: Methodology and Investigation; Minh Nguyet Nguyen: Data curation, Conceptualization, Writing – original draft; Nguyen Huu Huy Phuc, Thang Van Le: Reviewing and Supervision.

Declaration of competing interest. The authors declare that they have no known competing financial interests or personal relationships that could have appeared to influence the work reported in this paper.

REFERENCES

1. Wang D., Zhang X., Bao S., Zhang Z., Fei H., and Wu Z. - Phase engineering of a multiphasic 1T/2H MoS_2 catalyst for highly efficient hydrogen evolution, J. Mater. Chem. A **9** (6) (2017) 2681-2688. https://doi.org/10.1039/C6TA09409K.
2. Tang Q. and Jiang D.-e. - Mechanism of Hydrogen Evolution Reaction on 1T-MoS_2 from First Principles, ACS Catal. **6** (8) (2016) 4953-4961. https://doi.org/10.1021/acscatal.6b01211
3. Damien Voiry M. S., Silva R., Fujita T., Chen M., Asefa T., Shenoy Vivek B., Eda G., and Chhowalla M. - Conducting MoS_2 nanosheets as catalysts for hydrogen evolution reaction, Nano Lett. **13** (12) (2013) 6222-6227. https://doi.org/10.1021/nl403661s

4. Yang J., Wang K., Zhu J., Zhang C., and Liu T. - Self-Templated Growth of Vertically Aligned 2H-1T MoS_2 for Efficient Electrocatalytic Hydrogen Evolution, ACS Appl. Mater. Interfaces. **8** (46) (2016) 31702-31708. https://doi.org/10.1021/acsami.6b11298
5. Zhou Y. et al. - Rational design and synthesis of 3D MoS2 hierarchitecture with tunable nanosheets and 2H/1T phase within graphene for superior lithium storage, Electrochim. Acta. **211** (2016) 1048-1055. https://doi.org/10.1016/j.electacta.2016.06.123
6. Wu M. et al. - Metallic 1T MoS_2 nanosheet arrays vertically grown on activated carbon fiber cloth for enhanced Li-ion storage performance, J. Mater. Chem. A **5** (27) (2017) 14061-14069. https://doi.org/10.1039/C7TA03497K
7. Wang D., Xiao Y., Luo X., Z. Wu, Wang Y.-J., and Fang B. - Swollen Ammoniated MoS_2 with 1T/2H Hybrid Phases for High-Rate Electrochemical Energy Storage, ACS Sustain Chem Eng., **5** (3) (2017) 2509-2515. https://doi.org/10.1021/acssuschemeng.6b02863
8. Jiang L. et al. - Optimizing Hybridization of 1T and 2H Phases in MoS_2 Monolayers to Improve Capacitances of Supercapacitors, Mater. Res. Lett. **3** (4) (2015) 177-183. https://doi.org/10.1080/21663831.2015.1057654
9. Huang H. et al. - Metallic 1T phase MoS_2 nanosheets for high-performance thermoelectric energy harvesting, Nano Energy **26** (2016) 172-179. https://doi.org/10.1016/j.nanoen.2016.05.022
10. Hsiao M.-C. et al. - Ultrathin 1T-phase MoS_2 nanosheets decorated hollow carbon microspheres as highly efficient catalysts for solar energy harvesting and storage, J. Power Sources **345** (2017) 156-164. https://doi.org/10.1016/j.jpowsour.2017.01.132
11. Gigot A. et al. - Mixed 1T–2H Phase MoS_2/Reduced Graphene Oxide as Active Electrode for Enhanced Supercapacitive Performance, ACS Appl. Mater. Interfaces., **8** (48) (2016) 32842-32852. https://doi.org/10.1021/acsami.6b11290
12. Tang Q. and Jiang D.-e. - Mechanism of Hydrogen Evolution Reaction on 1T-MoS_2 from First Principles, ACS Catal. **6** (8) (2016) 4953-4961. https://doi.org/10.1021/acscatal.6b01211
13. Zhang Y., Kuwahara Y., Mori K., Louis C., and Yamashita H., - Hybrid phase 1T/2H-MoS_2 with controllable 1T concentration and its promoted hydrogen evolution reaction, Nanoscale **12** (22) (2020) 11908-11915. https://doi.org/10.1039/D0NR02525A
14. Geng X. et al. - Pure and stable metallic phase molybdenum disulfide nanosheets for hydrogen evolution reaction, Nat. Commun. **7** (1) (2016) 10672. https://doi.org/10.1038/ncomms10672
15. Lei Z., Zhan J., Tang L., Zhang Y., and Wang Y. - Recent Development of Metallic (1T) Phase of Molybdenum Disulfide for Energy Conversion and Storage, Adv. Energy Mater. **8** (19) 1703482 (2018). https://doi.org/10.1002/aenm.201703482
16. Liu Q. et al. - Gram-Scale Aqueous Synthesis of Stable Few-Layered 1T-MoS_2: Applications for Visible-Light-Driven Photocatalytic Hydrogen Evolution, Small **11** (41) (2015) 5556-5564. https://doi.org/10.1002/smll.201501822
17. Chen Y. X., Wu C. W., Kuo T. Y., Chang Y. L., Jen M. H., and Chen I. W. P. - Large-Scale Production of Large-Size Atomically Thin Semiconducting Molybdenum Dichalcogenide Sheets in Water and Its Application for Supercapacitor, Sci. Rep. **6** (1) (2016) 26660. https://doi.org/10.1038/srep26660

18. Ali M. E. M., Mohammed R., Abdel-Moniem S. M., El-Liethy M. A., and Ibrahim H. S. - Green MoS_2 nanosheets as a promising material for decontamination of hexavalent chromium, pharmaceuticals, and microbial pathogen disinfection: spectroscopic study, J Nanopart Res. **24** (10) (2022). https://doi.org/10.1007/s11051-022-05573-6
19. Pallikkarathodi Mani N. and Cyriac J. - Green approach to synthesize various MoS_2 nanoparticles via hydrothermal process, Bull. Mater. Sci., **45** (4) (2022). https://doi.org/10.1007/s12034-022-02757-7
20. Madani M. *et al*. - Green synthesis of nanoparticles for varied applications: Green renewable resources and energy-efficient synthetic routes, Nanotechnol. Rev. **11** (1) (2022) 731-759. https://doi.org/10.1515/ntrev-2022-0034
21. Priecel P. and Lopez-Sanchez J. A. - Advantages and Limitations of Microwave Reactors: From Chemical Synthesis to the Catalytic Valorization of Biobased Chemicals, ACS Sustain Chem Eng. **7** (1) (2019) 3-21. https://doi.org/10.1021/acssuschemeng.8b03286
22. Dong H., Chen Y. C., and Feldmann C. - Polyol synthesis of nanoparticles: status and options regarding metals, oxides, chalcogenides, and non-metal elements, Curr. Green Chem. **17** (8) (2015) 4107-4132. https://doi.org/10.1039/C5GC00943J
23. Collins T. J. - Review of the twenty-three year evolution of the first university course in green chemistry: teaching future leaders how to create sustainable societies, J. Clean. Prod. **140** (2017) 93-110. https://doi.org/10.1016/j.jclepro.2015.06.136
24. Castillo-Henriquez L., Alfaro-Aguilar K., Ugalde-Alvarez J., Vega-Fernandez L., Montes de Oca-Vasquez G., and Vega-Baudrit J. R. - Green Synthesis of Gold and Silver Nanoparticles from Plant Extracts and Their Possible Applications as Antimicrobial Agents in the Agricultural Area, Nanomaterials (Basel) **10** (9) (2020). https://doi.org/10.3390/nano10091763
25. Waskito I. S., Kurniawan B., Amal M. I., and Hanifuddin M. - The Effect of Precursors Concentration on the Structural Properties of MoS_2 Nanosheet-Microsphere Synthesized Via Hydrothermal Route, IOP Conf. Ser. Mater. Sci. Eng. **546** (2019). http://dx.doi.org/10.1088/1757-899X/546/4/042048
26. Wang F., Li G., Zheng J., Ma J., Yang C., and Wang Q. - Hydrothermal synthesis of flower-like molybdenum disulfide microspheres and their application in electrochemical supercapacitors, RSC Adv. **8** (68) 92018) 38945-38954. https://doi.org/10.1039/C8RA04350G
27. Suo Xia Hou C. W., Jie Huo Y. - Controllable Preparation of Nano Molybdenum Disulfide by Hydrothermal Method, Ceram. - Silik., **61** (2) (2017) 158 - 162, 2017. https://doi.org/10.13168/cs.2017.0011
28. Saber M., Khabiri G., Khabiri A. M., Ulbricht M., Khalil A., and M. R - A comparative study on the photocatalytic degradation of organic dyes using hybridized 1T/2H, 1T/3R and 2H MoS_2 nano-sheets, RSC Adv. **8** (2018) 26364-26370. https://doi.org/10.1039/C8RA05387A
29. Saseendran S. B., Ashok A., and A. A S - Edge terminated and interlayer expanded pristine MoS_2 nanostructures with 1T on 2H phase, for enhanced hydrogen evolution reaction, Int. J. Hydrogen Energy. **47** (16) (2022) 9579-9592. https://doi.org/10.1016/j.ijhydene.2022.01.031

30. Das S., Swain G., and Parida K. - One step towards the 1T/2H-MoS_2 mixed phase: a journey from synthesis to application, Mater. Chem. Front. **5** (5) (2021) 2143-2172. https://doi.org/10.1039/D0QM00802H
31. Das S., Swain G., and Parida K. - One step towards the 1T/2H-MoS_2 mixed phase: a journey from synthesis to application, Mater. Chem. Front. **5** (5) (2021) 2143-2172. https://doi.org/10.1039/D0QM00802H
32. Wang H. W., Skeldon P., and Thompson G. E. - XPS studies of MoS_2 formation from ammonium tetrathiomolybdate solutions, Surf. Coat. Int. **91** (3) (1997) 200-207. https://doi.org/10.1016/S0257-8972(96)03186-6
33. John F. Moulde W. F. S., Peter E. S., Kenneth Bomben D. - Handbook of X-ray photoelectron spectroscopy, 1992
34. Cheng P., Sun K., and Hu Y. H. - Memristive Behavior and Ideal Memristor of 1T Phase MoS_2 Nanosheets, Nano Lett. **16** (1) (2016) 572-576. https://doi.org/10.1021/acs.nanolett.5b04260
35. Hou M. et al. - Aging mechanism of MoS_2 nanosheets confined in N-doped mesoporous carbon spheres for sodium-ion batteries, Nano Energy **62** (2019) 299-309. https://doi.org/10.1016/j.nanoen.2019.05.048
36. Gao X., Xiong L., Wu J., Wan J., and Huang L. - Scalable and controllable synthesis of 2D high-proportion 1T-phase MoS_2, Nano Research **13** (11) (2020) 2933-2938. https://doi.org/10.1007/s12274-020-2950-2
37. Xin X. et al. - In-situ growth of high-content 1T phase MoS_2 confined in the CuS nanoframe for efficient photocatalytic hydrogen evolution, Appl. Catal. B: Enviro. **269** (2020) 118773. https://doi.org/10.1016/j.apcatb.2020.118773
38. Feng D., Pan X., Xia Q., Qin J., Zhang Y., and Chen X. - Metallic MoS_2 nanosphere electrode for aqueous symmetric supercapacitors with high energy and power densities, J. Mater. Sci. **55** (2020) 1-11. https://doi.org/10.1007/s10853-019-03997-5
39. Yu Y. et al. - High phase purity 1T'-MoS2 and 1T'-MoSe2 layered crystals, Nat. Chem. **10** (6) (2018) 638-643. https://doi.org/10.1038/s41557-018-0035-6
40. Wei J. *et al.* - Synthesis of Few Layer Amorphous 1T/2H MoS_2 by a One-Step Ethanol/Water Solvothermal Method and Its Hydrodesulfurization Performance, Catal. Letters **152** (1) (2021) 263-275. https://doi.org/10.1007/s10562-021-03621-9
41. Wang S., Luo Y., Fan Y., Ali A., Liu Z., and Kang Shen P. - Uniformly distributed 1T/2H-MoS_2 nanosheets integrated by melamine foam-templated 3D graphene aerogels as efficient polysulfides trappers and catalysts in lithium-sulfur batteries, J. Electroanal.Chem. **909** (2022). https://doi.org/10.1016/j.jelechem.2022.116099
42. Agrawal A. V. et al. - Controlled Growth of MoS_2 Flakes from in-Plane to Edge-Enriched 3D Network and Their Surface-Energy Studies, ACS Appl. Nano Mater. **1** (5) (2018) 2356-2367. https://doi.org/10.1021/acsanm.8b00467
43. Kim J. S. *et al.* - Electrical Transport Properties of Polymorphic MoS_2, ACS Nano, **10** (8) (2016 7500-7506. https://doi.org/10.1021/acsnano.6b02267
44. Lee Y. B. et al. - Facile microwave assisted synthesis of vastly edge exposed 1T/2H-MoS_2 with enhanced activity for hydrogen evolution catalysis, J. Mater. Chem. **7** (8) (2013) 3563-3569. https://doi.org/10.1039/C8TA12080C

45. Cai L. *et al.* - High-Content Metallic 1T Phase in MoS_2-Based Electrocatalyst for Efficient Hydrogen Evolution, J. Phys. Chem. C **121** (28) (2017) 15071-15077,. https://doi.org/10.1021/acs.jpcc.7b03103
46. Guo X., Wang Z., Zhu W., and Yang H. - The novel and facile preparation of multilayer MoS2 crystals by a chelation-assisted sol–gel method and their electrochemical performance, RSC Adv. 7 (15) (2017) 9009-901. https://doi.org/10.1039/C6RA25558B
47. Wojnarowicz J. et al. - Effect of Water Content in Ethylene Glycol Solvent on the Size of ZnO Nanoparticles Prepared Using Microwave Solvothermal Synthesis, J. Nanomater. **2016** (2016) 1-15. https://doi.org/10.1155/2016/2789871
48. Zheng Y. et al. - The effect of lithium adsorption on the formation of 1T-MoS2 phase based on first-principles calculation, Phys. Lett. A **380** (20) (2016) 1767-1771. https://doi.org/10.1016/j.physleta.2016.03.009